Dalton Transactions

X-ray absorption spectra of f-element complexes: Insight from relativistic multiconfigurational wavefunction theory

Journal:	*Dalton Transactions*
Manuscript ID	DT-FRO-12-2021-004075
Article Type:	Frontier
Date Submitted by the Author:	02-Dec-2021
Complete List of Authors:	SERGENTU, Dumitru-Claudiu; State University of New York at Buffalo, Chemistry Autschbach, Jochen; State University of New York at Buffalo, Chemistry

X-ray absorption spectra of f-element complexes: Insight from relativistic multiconfigurational wavefunction theory

Dumitru-Claudiu Sergentu[a] and Jochen Autschbach[a,*]

[a]Department of Chemistry
University at Buffalo
State University of New York
Buffalo, NY 14260-3000, USA
email: jochena@buffalo.edu

December 29, 2021

Abstract

X-ray absorption near edge structure (XANES) spectroscopy, coupled with ab-initio calculations, has emerged as the state-of-the-art tool for elucidating the metal-ligand bonding in f-element complexes. This highlight presents recent and on-going efforts in calculating XANES spectra of lanthanide and actinide compounds with relativistic multiconfiguration wavefunction approaches that account for differences in donation bonding in the ground state (GS) versus a core-excited state (ES), multiplet effects, and spin-orbit-coupling. With the GS and ES wavefunctions available, including spin-orbit effects, an arsenal of chemical bonding tools that are popular among chemists can be applied to rationalize the observed intensities in terms of covalent bonding.

1 Introduction

Research of the physico-chemical properties of compounds containing lanthanide (Ln) or actinide (An) elements is rapidly evolving in response to the urgent need for exploring the extent of f-shell chemical bonding in a variety of applications.[1–11] With radially compact 4f orbitals, Ln chemistry is dominated by the +III oxidation state, with +II and +IV being important variations.[12–15] Prior to Cm, actinide chemistry is characterized by a large variety of oxidation states.

The more diffuse valence metal 5d/6d shell is responsible for most of the covalent bonding in Ln/An complexes. Covalent bonding involving the Ln 4f orbitals has long been considered to be of minor importance, but there are notable exceptions. The 4f orbitals contribute to covalent bonding, e.g., in CeO_2, $Ce(C_8H_8)_2$, and other Ce(IV) systems,[16–23] NPrO,[24] PrO_2^+,[25] TbO_2 and PrO_2,[26] and $(C_5Me_5)_2Yb$.[27] 5f-shell bonding can be pronounced, especially for elements up to

Cm. Along the Ln/An row, the 4f/5f orbitals contract and become lower in energy, as a result of the incomplete nuclear charge screening among same-shell electrons. Toward the end of the rows, the f shells are core-like.

In order to advance applications of f-element chemistry, it is extremely important to be able to probe f- and d-shell covalency reliably by experiment and theory. X-ray absorption near-edge structure (XANES) spectroscopy has emerged as a preferred tool for probing sensitively the local electronic structure of coordinated Ln and An ions. When combined with ab-initio calculations, XANES is able to reveal the metal oxidation state, the local coordination symmetry, and the extent of covalent donation bonding. It is familiar to chemists that covalent bonding manifests itself in calculations via the mixing of overlapping atomic orbitals (AOs) of neighboring atoms in the molecular orbitals (MOs) in a way that is accompanied by constructive quantum interference and energetic stabilization of the system.[28,29] Furthermore, it is textbook knowledge that the mixing of AOs and the (de)stabilization of the (anti)bonding MO is larger when the AOs match well energetically, as compared to the case when the AOs have very different energies. Because the transitions probed in X-ray spectroscopy of metal complexes are out of strongly localized atomic core shells, the pre-edge intensities can be very sensitive to the extent of donation bonding.

The relation of the observed spectra with bond properties was rationalized by Hedman, Solomon and coworkers in a series of studies of transition metal complexes.[30–34] The same analysis is commonly applied to f-element complexes. Take, for example, a p-block ligand K-edge XANES experiment for an An complex. The spectrum is dominated by electric dipole-allowed transitions from the ligand 1s core orbital to virtual molecular MOs with ligand *n*p character. Pre-edge features may arise due to hybridized MOs with ligand *n*p and metal 5f or 6d antibonding character. The intensity and energetic splitting of the pre-edge peaks can then be rationalized by the amount of metal-ligand AO mixing in the acceptor MOs, the ligand-field (LF) splitting, and the extent of electron-electron repulsion between the added valence electron and existing metal valence electrons. Examples of Ln and An systems interrogated so far by ligand K-edge XANES are $M(C_8H_8)_2$ (M = Ce, Th, U),[35,36] MO_2 (M = Ce, Pr, Tb),[26] $[MCl_6]^{2-}$ (M = Ce, Th, U–Pu),[17,37,38] an $[MCl_6]^{3-}$ (M = Ce, Nd, Sm–Gd, Am).[17,39] In the early f-block, metal valence f and ligand valence AOs may become quasi-degenerate[40] while overlapping significantly. Consequently, there is potential for an interesting interplay between the AO energies and their overlap influencing the bonding for complexes of these elements. Much emphasis has in recent years been placed on the degeneracy aspect,[11,38,41–45] but it has also been pointed out repeatedly that AO energy degeneracy alone is not associated with covalent bonding as commonly understood by chemists.[46–51]

XANES at the metal L_3 and $M_{4,5}$ edges is also used in Ln and An chemistry research.[26,36,52–65] The L_3 edge probes dipole-allowed 2p → *n*d transitions. The (relative) intensity between the spectral features, and the energy of the main edge, is very sensitive to the metal oxidation state and f-electron count. The dipole-allowed transitions generating intensity in metal $M_{4,5}$ edges are 3d → *n*f. In this case, the intensity and energy splitting between the spectral features bear information on the LF splitting of the f-orbitals and thus, at least in theory, they provide direct evidence of f-orbital covalency.[58] In practice, spin-orbit (SO) coupling and multiplet effects lead to broadening and re-distribution of intensity among the L_3 and $M_{4,5}$ edge features to the extent that rationalization of f-orbital covalency becomes a complex task even with support from ab-initio calculations. Among the Ln and An systems that have been interrogated by metal L_3 and

$M_{4,5}$ XANES, CeO_2,[26,52,53,60,66–69] $Ce(C_8H_8)_2$[54,69,70] and $[MO_2]^{2+}$ (M = U–Pu)[58,71] are notable because they are representative of the intricate f-orbital covalent bonding scenarios that may occur in general lanthanide and actinide compounds.

The experimentally observed intensities, in XANES and other types of electronic spectroscopy, probe the GS and the ES simultaneously, via the transition moments. Therefore, a theoretical model is required for a useful interpretation of the spectra in terms of ground state bonding. There has been significant progress in recent years, regarding the accurate calculation and interpretation of XANES spectra of f-element complexes by virtue of relativistic multiconfiguration wavefunction theory (MC-WFT). This is important because the aforementioned interpretation of XANES spectra relies, implicitly or explicitly, on calculated MOs that are assumed to be the same for the GS and an ES. This is an approximation that may or may not be suitable, depending on the system. Furthermore, efficient one-electron theories used for XANES simulations are inadequate to treat the multireference states encountered in much of f-element chemistry, or the multiplet and SO effects in XANES, as discussed in the following section.

2 Computational tools for XANES calculations

There are a number of different computational approaches for XANES, some trading accuracy or the level of insight that can be gained for speed, or vice versa. Finite difference methods and multiple scattering approaches[72–75] proved to be fast and reliable in predicting spectra for a variety of An complexes.[58,59,64,76–80] Other techniques used for Ln/An XANES are the static-exchange approximation,[81–83] the charge-transfer and atomic-multiplet model,[26,36,84] and atomic multiplet approaches with wavefunctions obtained self-consistently in four-component Dirac Hartree-Fock calculations.[58,85,86] Computationally feasible and much preferred by the chemistry community are MO-based DFT approaches,[87] such as time-dependent DFT (TDDFT) or the GS transition-dipole DFT approach.[35,38,39,83,88,89] DFT-based restricted open-shell configuration-interaction with singles (ROCIS) has also been used to calculate XANES of transition metal systems[90–95] but, to our knowledge, not yet for f-element XANES.

DFT approaches invoke two approximations that are important to mention regarding XANES calculations for heavy element complexes. First, Kohn-Sham DFT uses a single Slater determinant for the ‘noninteracting system’ to describe the GS. Second, the electron correlation in the GS and a core-ES are prone to differ. This can be re-cast as an orbital relaxation upon excitation, which means a compact description of the ES may need somewhat different orbitals than the most compact description of the GS. Neither TDDFT, as commonly applied in XANES calculations, nor transition-dipole DFT account for this orbital relaxation. At least in principle, both these approximations may be severe. The electronic states of f-element complexes tend to be severely multiconfigurational, and final state effects may dictate the spectral profile.[26,54,60,69,70]

Approaches based on a multiconfiguration *ansatz* for the wavefunction, with orbital optimization, are demanding of computational resources and typically not of a ‘black box’ type. Nonetheless, this approach is attractive for calculating XANES spectra. Obvious reasons are that multiconfigurational states and ES orbital relaxation can be treated. WFT, in principle, also allows for a systematic improvement of the electron correlation treatment. The SO interaction can either be treated variationally, by means of using two- or four-component orbitals from which the configurations are built, or it can be treated via interaction of scalar relativistic, so-called spin-free

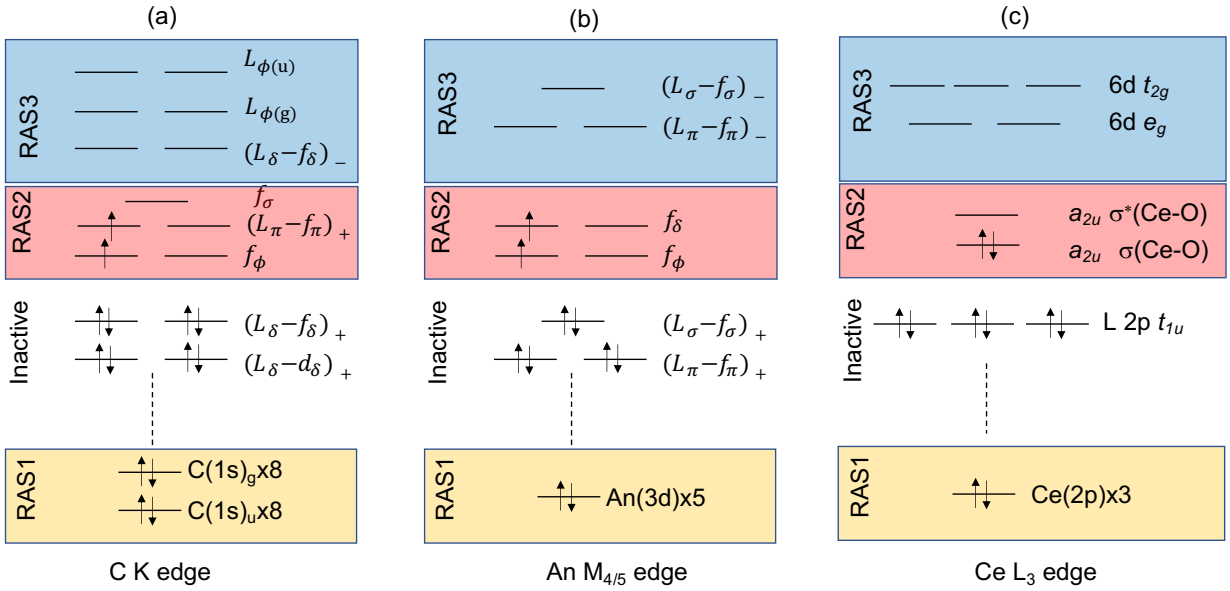

Figure 1: Schematic illustration of the restricted active space selection for calculating (a) the C K-edge of $U(C_8H_8)_2$,[116] (b) the Pu $M_{4/5}$ edges of PuO_2^{2+},[71] and (c) the Ce L_3 edge of CeO_2.[69]

(SF), many-electron states belonging to a given spin multiplicity. Such approaches, described in detail in recent reviews,[96–98] met with significant success in calculations of XANES and resonant inelastic X-ray scattering (RIXS) maps for a variety of transition metal complexes.[99–113,113–115]

3 An and Ln XANES with multiconfiguration wavefunction theory

MC-WFT XANES calculations for f-element systems have relied on the active space self-consistent field (SCF) method[117–119] with state-interaction treatment of the SO coupling. The approach was recently also used for calculating uranyl 3d→4f RIXS.[120]

In the complete active space SCF (CASSCF) approach, a set of active orbitals is selected along with a number of electrons. Full configuration interaction (CI) is then performed within this active space, while keeping other orbitals and electrons inactive. SCF pertains to a minimization of the state energy, or the average energy of a set of states in state-averaged CASSCF, with respect to the active and inactive orbitals. In the restricted active space (RAS) approach, there are three active spaces, RAS1/2/3. The electron occupancy in RAS2 is unrestricted. RAS1/3 is characterized by a maximum number of electron holes/electrons. Thus, RAS can be viewed as a restriction on a CAS that spans the combined RAS1/2/3 spaces.

For XANES, an obvious setup is that the core orbitals with at most one electron hole allowed constitute RAS1. Valence MOs that are relevant for the studied XANES process constitute RAS2 and RAS3. The computational demand of active space methods scales exponentially or worse with the size of the active spaces. Thus, the number of valence and core-excited wavefunctions that need to be calculated quickly become intractable with the number of electrons and MOs correlated in RAS2 particularly, for which critical but relevant choices have to be made. Ex-

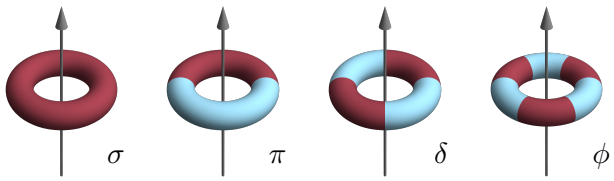

Figure 2: From left to right, the coloring pattern of the torus indicates the nodal patterns for orbitals with σ, π, δ, and ϕ symmetry, respectively, with respect to a symmetry axis.

amples of RAS choices that have been used to calculate various edges in Ln and An complexes are illustrated in Figure 1. The state energies may be corrected for the dynamic correlation, for instance via multireference second-order perturbation theory (PT2).[121–125] RAS state interaction (RASSI)[126] is then used to introduce the SO coupling. Electric-dipole oscillator strengths, and magnetic-dipole and electric-quadrupole contributions if necessary, needed to generate the XANES spectrum, can be determined either from the SF or SO states, to assess the impact of SO coupling.

With recent modifications of the RASSI property code[127–130] of OpenMolcas,[131,132] spin-independent natural orbitals (NOs) and natural spin orbitals, and their populations, can be calculated for any desired valence or core-excited SO state, which greatly facilitates the analysis of the XANES intensities. Moreover, a Python code project recently developed by some members of our group, *eXatomic*,[133] can generate input files for the popular natural bond orbital (NBO)[134] program from both SF and SO RASSI wavefunctions, facilitating the analysis of XANES intensities in terms of the metal-ligand bonding captured in natural localized molecular orbitals (NLMOs),[134,135] and in terms of bond orders and other analysis offered by the NBO algorithms. Additionally, electronic states under the XANES peaks may be interpreted with the help of the popular and compact natural transition orbital (NTO) representation,[136–138] which can be generated from multiconfigurational SF[139] and SO[140] wavefunctions. Therefore, one can apply a variety of popular chemical-bonding tools to the GS and ES wavefunctions, to rationalize the complex X-ray near-edge structures of Ln and An complexes. In the following sections, we give examples of metal and ligand XANES calculations for selected f-element complexes performed by us.

4 Carbon K-edge XANES of actinocenes

In Reference 116, the C K-edge XANES spectra in $An(C_8H_8)_2$, An = Th[141] and U,[142] (transitions from 1s to valence p transitions) were calculated with RAS approaches and compared with available experiments.[35] In addition to many other interesting electronic structure features of these two actinocenes,[35,143–146] the interpretation of the C K-edge measurements with TDDFT transition densities and GS Kohn-Sham orbitals was initially thought to provide evidence of ϕ-symmetry actinide-ligand covalency, in addition to the widely known 5f and 6d δ-symmetry donation bonding mechanism.[35] The symmetry classification is in reference to the nodal patterns of the metal and ligand orbitals with respect to the principal axis of symmetry, as sketched in Fig-

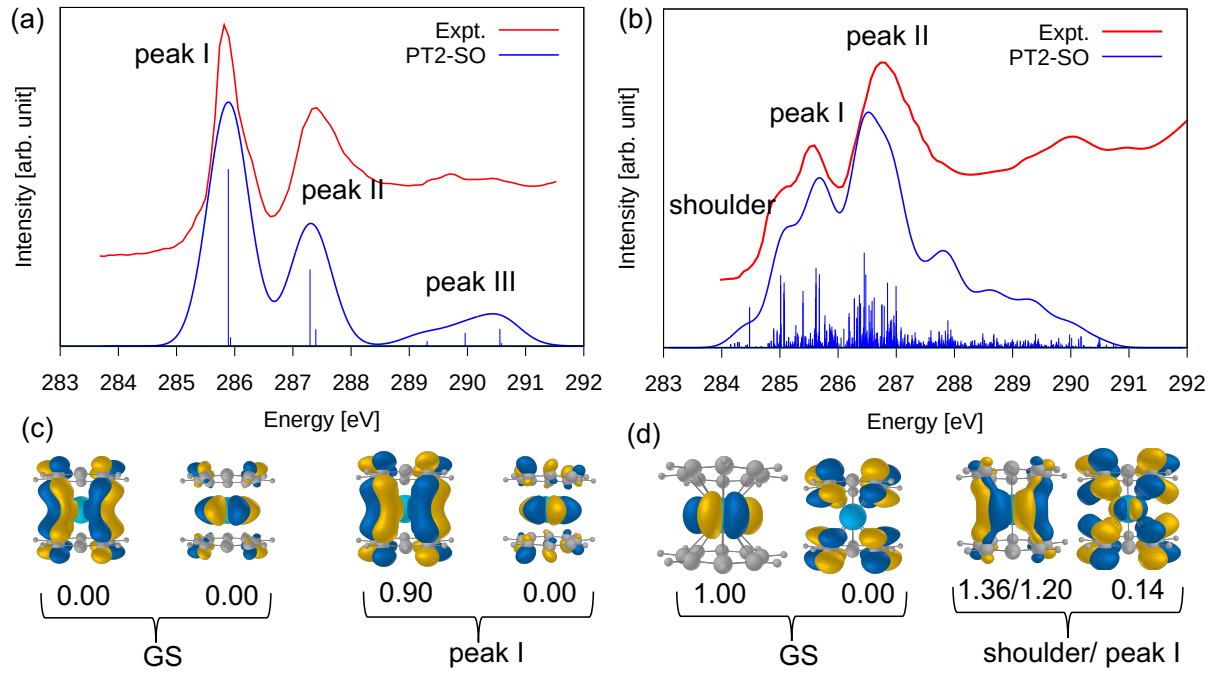

Figure 3: C K-edge XANES in $An(C_8H_8)_2$, An = Th (panel a) and U (panel b). The active space selection is shown in Fig. 1. Panels d (An = Th) and e (An = U) show isosurface plots of the ϕ_u-symmetry NOs and their occupations in the GS and in one of the most intense core ESs of the shoulder/peak I features. Theoretical data from Ref. 116. Experimental data from Ref. 35.

ure 2. Although it is uncontested that $Th(C_8H_8)_2$ shows metal-ligand 5f ϕ-symmetry mixing,[145] it only appears in the unoccupied GS orbitals and was proven to have no influence on the chemical reactivity of the complex.[147] [This is in contrast, for example, to An complexes with metallacyclopropenes and metallacyclocumulenes (An=Pa–Pu) where ϕ back-bonding contributes to lengthening of the An–C bonds from Pa to Pu.[148]] Consequently, the net ϕ-symmetry effective bond order (EBO)[149] is strictly nil for $Th(C_8H_8)_2$ in its GS. For uranocene, one unpaired electron populates the two $5f_\phi$ orbitals such that, at least in principle, GS ϕ back-donation becomes a possibility. However, the U $5f_\phi$ shell is well separated energetically from the lowest unoccupied ligand orbital combination of ϕ_u symmetry. Combined with relatively weak overlap, this means that ϕ bonding in $U(C_8H_8)_2$ is also essentially absent in the GS.

The MC-WFT calculations and analysis of the XANES established clear evidence of 5f ϕ bonding in the excited states of thorocene and uranocene, and more recently[89]—more enhanced yet—ϕ bonding in the core-ESs of $[U(C_7H_7)_2]^-$. Thorocene features a sharp intense low energy peak in the carbon K-edge spectrum (peak I in Figure 3a) associated with core transitions into ϕ_u MOs with in-phase metal-ligand mixing. This peak becomes broader, loses intensity, and is preceded by a shoulder in the uranocene spectrum (Figure 3b), which may indicate that the C 2p weights in these ϕ_u MOs dropped significantly. Our study[116] confirmed the hypothesis that ϕ-symmetry covalent bonding in $An(C_8H_8)_2$ with An = Th, U, should be regarded as a characteristic of the spectroscopically probed core ESs governing the intensity of peaks I of the C K-edge

spectra.

The isosurface plots of the metal-ligand in-phase bonding and out-of-phase antibonding NOs of ϕ_u symmetry, extracted from the most intense core ESs of peaks I/shoulder of each complex, are shown in panels c and d of Figure 3. For thorocene, the NOs show that compared to the GS the metal 5f - ligand 2p ϕ mixing is slightly enhanced in the core ES, and the bonding NOs are occupied. This yields ES ϕ covalency with an EBO of 0.45. The ϕ_u NOs are even more interesting for uranocene, because they show negligible metal-ligand mixing for the GS but sizable mixing for the core ES (Figure 3d). An important aspect to notice from Figure 3c and 3d is that the lower-energy ϕ_u MOs with in-phase metal-ligand mixing are ligand-centered in thorocene but metal-centered in uranocene, which rationalizes the reduction of shoulder/peak I intensity going from Th to U and is clear evidence of ϕ bonding in the uranocene ESs. Broadening in the shoulder/peak I of uranocene is additionally caused by intra-shell Coulomb repulsion between the added core electron and the existing $5f^1_\phi$ electron, and the intense core ESs under the whole K-edge envelope are strongly multiconfigurational such that contributions from individual 5f-based MOs cannot be singled-out for each peak.

In the case of thorocene, peaks I and II occur due to core transitions into the unoccupied ligand ϕ_u and ϕ_g combinations, respectively, split energetically by the presence of Th^{4+}. This aspect was confirmed in Ref. 116 by comparison with the peak-structure of a ligand-only $(C_8H_8)_2^{4-}$ model. Additional calculations that did not include the metal 5f basis functions produced peaks I and II, but not peak III. Peak III rises in intensity due to metal-ligand antibonding ϕ_u combinations in the full complex from ES ϕ bonding.

5 Actinide $M_{4/5}$-edge XANES of AnO_2^{2+}

In Reference 71, the U M_4 edge of UO_2^{2+} and the Np and Pu M_5 edges of NpO_2^{2+} and PuO_2^{2+}, respectively, were calculated with relativistic MC-WFT and analyzed. Experiments and other types of calculations were previously reported by Vitova et al.[58] The M edges probe actinide centered 3d→5f transitions.

The electronic structure of the linear actinyl systems is particularly interesting because the 5f σ and π AOs form short bonds with the 2p AOs of the axial ('yl') oxygens. The strong bonding is acknowledged in particular for uranyl, where it is enhanced by a 'pushing from below' mechanism.[150–153] The latter implies an electrostatic repulsion of the uranium $6p_\sigma$ semi-core AO by the electron-rich bonding environment, leading to hybridization with 5f in the σ U–O_{yl} MO and and pushing it energetically above the π U–O_{yl} MOs. The An–O axial bonds contract slightly from UO_2^{2+} to PuO_2^{2+}. The contraction was proven to be driven by the decrease in the ionic radius.[154–156] Other studies indicated increasing 5f covalency in the An–O_{yl} bonds toward Pu.[157–159]

Calculated and experimental XANES spectra are shown in Figure 4. The agreement is excellent. The U M_4 edge shows a main peak assigned to transitions to nonbonding 5f ϕ and δ, a shoulder from transitions to U–O antibonding orbitals with 5f π character, and a satellite assigned to transitions to 5f σ antibonding orbitals. Going from U to Pu, the 5f ϕ, δ and π transitions merge under a single peak, and the energetic separation to the 5f σ satellite becomes smaller. If the main peak-satellite splitting reflects the σ-σ^* splitting of the MOs in the GS and thus the magnitude of the σ bond covalency, and if the merging of π transitions into the main peak reflects a decreasing

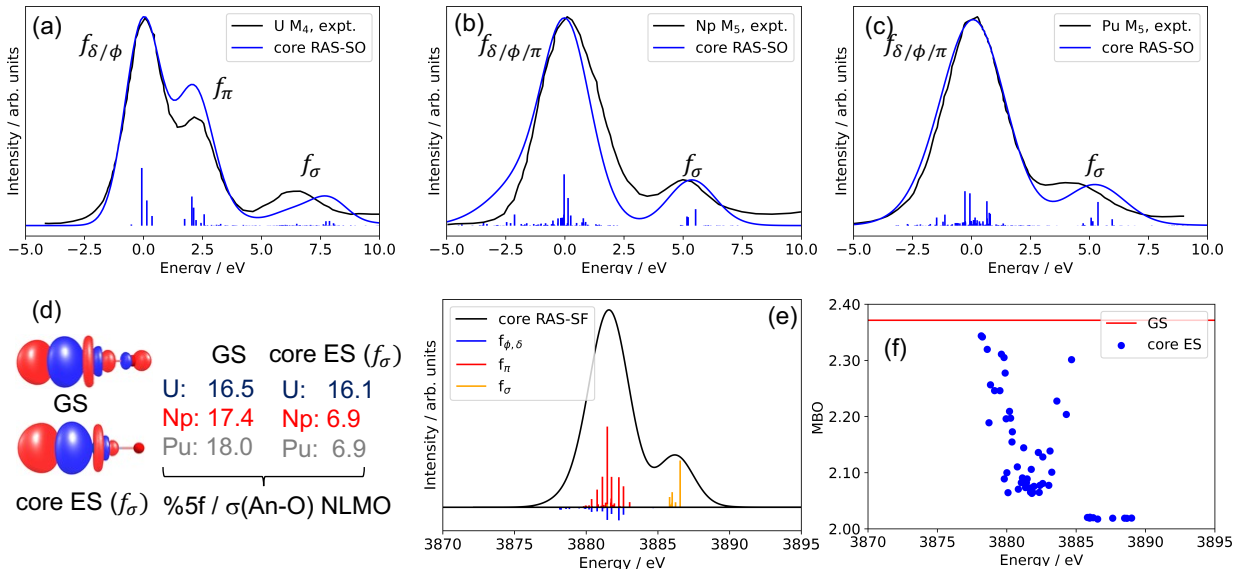

Figure 4: Metal $M_{4/5}$-edge XANES in AnO_2^{2+}, An = U (a), Np (b) and Pu (c). (d) Isosurface plots of representative σ(An–O) NLMOs, and their %5f weights, in the GS vs. the most intense core ES of the f_σ peak for each system. The NLMOs shown are those of PuO_2^{2+}. (e) Calculated spin-free Pu M-edge spectrum. The 'sticks' represent oscillator strengths scaled by the population of the different NOs with An 5f character in the core ESs. For better visual separation only, the 5f π indicators are drawn with negative sign. (f) Mayer bond orders calculated for the GS vs. intense core ESs generating intensity in the spin-free Pu M edge spectrum. Theoretical data from Ref. 71 and present work. Experimental data from Ref. 58.

π-π^* MO splitting in the GS, then the trends in the spectra must be interpreted as decreasing 5f GS covalency from U to Pu, especially for the σ bonds. Our analysis of the GS and ES wavefunctions shows that 5f covalency increases from U to Pu in the GSs, in agreement with several previous studies.[157–159] However, 5f covalency decreases from U to Pu in the σ^* core-ESs that cause the satellite peak's intensity. This means that the decreasing energy offset of the satellite peak informs about the 5f covalency trend in the σ^* ESs and not in the GSs. The conclusion is supported by NLMO metal-ligand bonding analyses of the relevant wavefunctions (see Figure 4, panel d).

Figure 4e additionally shows the SF spectrum of PuO_2^{2+} and its assignment in terms of core transitions into the metal 5f orbitals. The Pu–O Mayer bond order (MBO) for each state is compared with the GS MBO in Figure 4f. For the states under the σ^* satellite, the MBO is reduced by 0.35 on average, reflecting the occupation of the σ_u^* orbitals in the excited state as well as orbital relaxation. In other words, because the GS plutonyl(VI) σ bonds are so strongly 5f bonding, when the strongly antibonding orbitals become occupied in the ES, the system can stabilize by a reduction in the 5f covalency. Results like these depend on the specific system being studied and should not be generalized. For example, very recent calculations of the Pu $M_{4,5}$ edges of PuO_2 suggested quite localized Pu 5f orbitals without significant changes between the GS and the core ESs.[86]

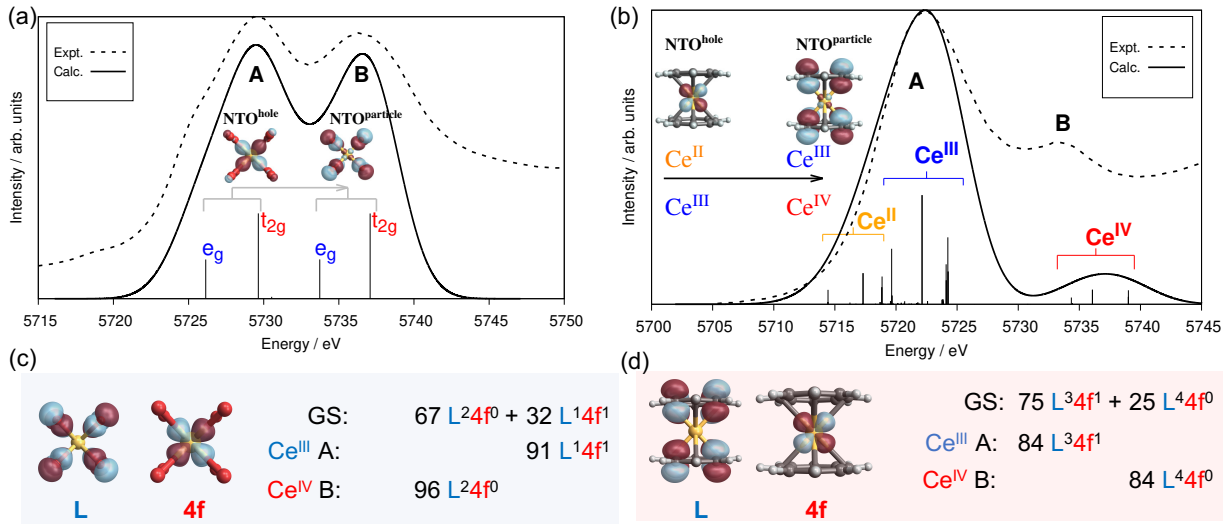

Figure 5: Ce L_3-edge XANES of CeO_2 (a) and $Ce(C_8H_8)_2$ (b). Panels c (CeO_2) and d ($Ce(C_8H_8)_2$): Wavefunction expressions for the GS and most intense core ESs in the basis of localized orthonormal Ce 4f and ligand (L) O 2p AO combinations. In the perspective used for the visuals, half of the orbital lobes are hidden. Theoretical data from Ref. 69. Experimental data from Refs. 26 and 54.

6 Ce L_3-edge XANES in CeO_2 and $Ce(C_8H_8)_2$

Cerium L_3-edge XANES (2p→5d transitions) MC-WFT calculations were reported in Ref. 69. Solid ceria (CeO_2), and cerocene [$Ce(C_8H_8)_2$], have long been used as representatives for the different appearances of the double-peaked L_3 edge shown in Figure 5, and its interpretation in terms of the controversial +III vs. +IV cerium oxidation number (ON).[26,36,54,70,146,160–168] The calculations for CeO_2 were performed with a charge-embedded $[CeO_8]^{12-}$ cluster model. As seen in Figure 5, the MC-WFT calculations reproduce the L_3 edge peaks very well.

The interpretation of the spectra, and indeed the assignment of the metal ON,[18] is fraught with complications because of three aspects. First, there are varying degrees of donation bonding, in particular in formal Ce(IV) systems, which blurs the distinction between the +III and +IV ONs. Second, in MC-WFT calculations, the degree of donation bonding in a given cerium or any other complex may show up in the form of metal-ligand AO hybridization in the MOs of the active space, or by the presence of charge-transfer configurations in the wavefunction expressed in a basis of localized active-space orbitals. Third, the GS wavefunctions of cerium complexes may be genuinely multiconfigurational regardless of the active-space orbital basis in which they are expressed.

The spectroscopic assignment of the ON relies on the assumption that peak A (refer to Figure 5) represents comparatively clean Ce(III) $4f^1$ sub-configurations of the 2p→5d excited states, split by the 5d LF, whereas peak B represents comparatively clean Ce(IV) $4f^0$ sub-configurations. If this were the case, then a clean $4f^1$ or $4f^0$ GS would give intensity only for peak A or B, but not for both. The intensity ratio of the peaks can then be used to assess $4f^1/4f^0$ GS configurational mixing which effectively determines n_f, the 4f shell occupation, and by extension the ON.

When we analyzed the relationship between the peak A and B states with the help of 'hole' and 'particle' NTOs, as shown in the insets of Figure 5(a,b), an astonishingly clear picture emerged: Going from an ES under peak A to its counterpart under peak B, the NTOs give a clean 4f to ligand transition. For cerocene there were in fact 3 groups of states, each group related to the next group at higher energy by a 4f to ligand transition, such that the lower energy part of peak A is assigned to formal $4f^2$ Ce(II) sub-configurations.

Relevant $4f^1$ and $4f^0$ ESs and the GS are characterized in Figure 5(c,d) in terms of configurations arising from a common active space of metal or ligand localized MOs. In the basis of these MOs, most of the states are strongly multiconfigurational. For cerocene, $4f^1$ dominates in the GS and in the intense Peak A ESs, rationalizing the A:B intensity ratio of roughly 90:10. The resulting spectroscopic 4f-shell occupancy (n_f) of 0.9 supports the now accepted Ce^{III} assignment. We confirmed in our calculations previous findings by Dolg and coworkers[161,162,167] that no orthogonal transformation among the active space orbitals gives a single-configuration state. The GS of cerocene is multiconfigurational.

For CeO_2, the A:B peak intensity ratio is about 60:40, i.e. the spectroscopic n_f is 0.6.[26,53,60,168] To rationalize these intensities, the system has been argued to exhibit an intermediate-valent GS with nearly equal admixture of $4f^1$ and Ce^{IV} $4f^0$ configurations.[60,168] We emphasize that such an assignment depends on the chosen orbital basis and the assumption that the ESs are clean $4f^1$ and $4f^0$ sub-configurations, respectively. As seen in Figure 5(c), the GS in the maximally localized MO basis is a mixture of a dominant $4f^0$ (67% weight) with a secondary $4f^1$ configuration (32%). Unlike cerocene, an orthogonal transformation among the active space orbitals produces a single-configurational GS in which the ligand-centered orbitals (L) are doubly occupied but display significant in-phase mixing with the 4f AOs, especially in the a_{2u} species. (For details please see Ref. 69.) In other words, the 32% weight of the $4f^1$ configuration in the GS of CeO_2 comes from donation bonding and can alternatively be represented by a single-configuration state with valence ligand orbitals that are delocalized onto the metal. Both in the localized and in the a delocalized MO basis, the core-ESs have multiconfigurational character, which ultimately rationalizes the nearly equal A:B intensity ratio. It is also clear that the peak intensity ratio has its origin in the extent of donation bonding. The spectroscopic value n_f of about 0.6 is consistent with GS 4f shell populations extracted from quantum chemical calculations.

7 Outlook

Wavefunction theory methods for calculating core-valence transitions, determining the associated absorption and emission wavelengths & intensities, and analyzing the relevant electronic states in terms of chemical bonding, are producing important new insights in f-element chemistry. It is preferable to extract this insight by using a multiconfiguration ab-initio electronic structure method that treats the ligand field, the orbital relaxation upon excitation, and the spin-orbit coupling, and that is able to reproduce the experimental spectra satisfactorily. In this way, the calculation has a direct connection with the experimental data used to extract chemical bonding information. The type of calculation highlighted herein produces ground and excited state wavefunctions, which can be subjected to a variety of analyses aimed at extracting bond orders, metal charges, f- and d-shell populations, the electron density topology, and other properties for each state, as well as relationships between the GS and the ES, and between ESs, in terms of natural

transition orbitals. Of course, like in all practical calculations, approximations have to be made. With recent developments, quite advanced electronic structure approaches have emerged for theoretical X-ray absorption spectroscopy. Examples include recent extension of coupled-cluster singles and doubles (CCSD) approaches for calculating core excited states (ESs) of simple organic molecules,[169–173] and multireference configuration interaction (MRCI) and multireference coupled-cluster approaches for calculating L-edge spectra of transition metal complexes.[114] Such approaches are extremelly demanding of computational resources and have so far not been used to calculate core ESs in actinide and lanthanide systems.

Conflict of interest

There are no conflicts of interest.

Acknowledgments

We acknowledge financial support from the U.S. Department of Energy, Office of Basic Energy Sciences, Heavy Element Chemistry program, under grant DE-SC0001136, and thank the Center for Computational Research (CCR)[174] at the University at Buffalo for providing computational resources.

References

[1] P. L. Arnold, T. Ochiai, F. Y. Lam, R. P. Kelly, M. L. Seymour and L. Maron, *Nat. Chem.*, 2020, **12**, 654–659.

[2] S. K. Singh, C. J. Cramer and L. Gagliardi, *Inorg. Chem.*, 2020, 6815–6825.

[3] D. Shao and X.-Y. Wang, *Chin. J. Chem.*, 2020, **38**, 1005–1018.

[4] X. Zhang, W.-L. Li, L. Feng, X. Chen, A. Hansen, S. Grimme, S. Fortier, D.-C. Sergentu, T. J. Duignan, J. Autschbach, S. Wang, Y. Wang, G. Velkos, A. A. Popov, N. Aghdassi, S. Duhm, X. Li, J. Li, L. Echegoyen, W. H. E. Schwarz and N. Chen, *Nat. Commun.*, 2018, **9**, 2753.

[5] J. Zhuang, L. Abella, D.-C. Sergentu, Y.-R. Yao, M. Jin, W. Yang, X. Zhang, X. Li, L. Echegoyen, J. Autschbach and N. Chen, *J. Am. Chem. Soc.*, 2019, **141**, 20249–20260.

[6] Q. Meng, L. Abella, W. Yang, Y.-R. Yao, X. Liu, J. Zhuang, X. Li, L. Echegoyen, J. Autschbach and N. Chen, *J. Am. Chem. Soc.*, 2021, **143**, 16226–16234.

[7] W. Shen, S. Hu and X. Lu, *Chem. Eur. J.*, 2020, **26**, 5748–5757.

[8] A. Jaro, C. Foroutan-Nejad and M. Straka, *Inorg. Chem.*, 2020, **59**, 12608–12615.

[9] R. M. Pallares and R. J. Abergel, *Nanoscale*, 2020, **12**, 1339–1348.

[10] B. Sadhu, M. Dolg and M. S. KulkarniSadhu, *J. Comput. Chem.*, 2020, **41**, 1427–1435.

[11] M. L. Neidig, D. L. Clark and R. L. Martin, *Coord. Chem. Rev.*, 2013, **257**, 394–406.

[12] M. R. MacDonald, J. E. Bates, M. E. Fieser, J. W. Ziller, F. Furche and W. J. Evans, *J. Am. Chem. Soc.*, 2012, **134**, 8420–8423.

[13] M. R. MacDonald, J. E. Bates, J. W. Ziller, F. Furche and W. J. Evans, *J. Am. Chem. Soc.*, 2013, **135**, 9857–9868.

[14] M. E. Fieser, M. R. MacDonald, B. T. Krull, J. E. Bates, J. W. Ziller, F. Furche and W. J. Evans, *J. Am. Chem. Soc.*, 2015, **137**, 369–382.

[15] W. J. Evans, *Organometallics*, 2016, **35**, 3088–3100.

[16] J. A. Bogart, A. J. Lewis, S. A. Medling, N. A. Piro, P. J. Carroll, C. H. Booth and E. J. Schelter, *Inorg. Chem.*, 2013, **52**, 11600–11607.

[17] M. W. Löble, J. M. Keith, A. B. Altman, S. C. E. Stieber, E. R. Batista, K. S. Boland, S. D. Conradson, D. L. Clark, J. L. Pacheco, S. A. Kozimor, R. L. Martin, S. G. Minasian, A. C. Olson, B. L. Scott, D. K. Shuh, T. Tyliszczak, M. P. Wilkerson and R. A. Zehnder, *J. Am. Chem. Soc.*, 2015, **137**, 2506–2523.

[18] R. Anwander, M. Dolg and F. T. Edelmann, *Chem. Soc. Rev.*, 2017, **46**, 6697–6709.

[19] L. A. Solola, A. V. Zabula, W. L. Dorfner, B. C. Manor, P. J. Carroll and E. J. Schelter, *J. Am. Chem. Soc.*, 2017, **139**, 2435–2442.

[20] T. Cheisson, K. D. Kersey, N. Mahieu, A. McSkimming, M. R. Gau, P. J. Carroll and E. J. Schelter, *J. Am. Chem. Soc.*, 2019, **141**, 9185–9190.

[21] Y. Qiao, H. Yin, L. M. Moreau, R. Feng, R. F. Higgins, B. C. Manor, P. J. Carroll, C. H. Booth, J. Autschbach and E. J. Schelter, *Chem. Sci.*, 2021, **12**, 3558–3567.

[22] G. B. Panetti, D.-C. Sergentu, M. R. Gau, P. J. Carroll, J. Autschbach, P. J. Walsh and E. J. Schelter, *Nat. Commun.*, 2021, **12**, 1713 (7 pages).

[23] Y. Qiao, H. Yin, L. M. Moreau, R. Feng, R. F. Higgins, B. C. Manor, P. J. Carroll, C. H. Booth, J. Autschbach and E. J. Schelter, *Chem. Sci.*, 2021, **12**, 3558–3567.

[24] S.-X. Hu, J. Jian, J. Su, X. Wu, J. Li and M. Zhou, *Chem. Sci.*, 2017, **8**, 4035–4043.

[25] Q. Zhang, S.-X. Hu, H. Qu, J. Su, G. Wang, J.-B. Lu, M. Chen, M. Zhou and J. Li, *Angew.Chem. Int.Ed.*, 2016, **55**, 6896–6900.

[26] S. G. Minasian, E. R. Batista, C. H. Booth, D. L. Clark, J. M. Keith, S. A. Kozimor, W. W. Lukens, R. L. Martin, D. K. Shuh, S. C. E. S. Stieber, T. Tylisczcak and X. dong Wen, *J. Am. Chem. Soc.*, 2017, **139**, 18052–18064.

[27] C. H. Booth, M. D. Walter, D. Kazhdan, Y.-J. Hu, W. W. Lukens, E. D. Bauer, L. Maron, O. Eisenstein and R. A. Andersen, *J. Am. Chem. Soc.*, 2009, **131**, 6480–6491.

[28] D. S. Levine and M. Head-Gordon, *Nat. Commun.*, 2020, **11**, 1–8.

[29] S. Nordholm and G. B. Bacskay, *Molecules*, 2020, **25**, 2667.

[30] B. Hedman, K. O. Hodgson and E. I. Solomon, *J. Am. Chem. Soc.*, 1990, **112**, 1643–1645.

[31] S. E. Shadle, J. E. Penner-Hahn, H. J. Schugar, B. Hedman, K. O. Hodgson and E. I. Solomon, *J. Am. Chem. Soc.*, 1993, **115**, 767–776.

[32] S. E. Shadle, B. Hedman, K. O. Hodgson and E. I. Solomon, *J. Am. Chem. Soc.*, 1995, **117**, 2259–2272.

[33] T. Glaser, B. Hedman, K. O. Hodgson and E. I. Solomon, *Acc. Chem. Res.*, 2000, **33**, 859–868.

[34] M. L. Baker, M. W. Mara, J. J. Yan, K. O. Hodgson, B. Hedman and E. I. Solomon, *Coord. Chem. Rev.*, 2017, **345**, 182–208.

[35] S. G. Minasian, J. M. Keith, E. R. Batista, K. S. Boland, D. L. Clark, S. A. Kozimor, R. L. Martin, D. K. Shuh and T. Tyliszczak, *Chem. Sci.*, 2014, **5**, 351–359.

[36] D. E. Smiles, E. R. Batista, C. H. Booth, D. L. Clark, J. M. Keith, S. A. Kozimor, R. L. Martin, S. G. Minasian, D. K. Shuh, S. C. E. Stieber and T. Tyliszczak, *Chem. Sci.*, 2020, **11**, 2796–2809.

[37] S. G. Minasian, J. M. Keith, E. R. Batista, K. S. Boland, D. L. Clark, S. D. Conradson, S. A. Kozimor, R. L. Martin, D. E. Schwarz, D. K. Shuh, G. L. Wagner, M. P. Wilkerson, L. E. Wolfsberg and P. Yang, *J. Am. Chem. Soc.*, 2012, **134**, 5586–5597.

[38] J. Su, E. R. Batista, K. S. Boland, S. E. Bone, J. A. Bradley, S. K. Cary, D. L. Clark, S. D. Conradson, A. S. Ditter, N. Kaltsoyannis, J. M. Keith, A. Kerridge, S. A. Kozimor, M. W. Löble, R. L. Martin, S. G. Minasian, V. Mocko, H. S. L. Pierre, G. T. Seidler, D. K. Shuh, M. P. Wilkerson, L. E. Wolfsberg and P. Yang, *J. Am. Chem. Soc.*, 2018, **140**, 17977–17984.

[39] J. N. Cross, J. Su, E. R. Batista, S. K. Cary, W. J. Evans, S. A. Kozimor, V. Mocko, B. L. Scott, B. W. Stein, C. J. Windorff and P. Yang, *J. Am. Chem. Soc.*, 2017, **139**, 8667–8677.

[40] J.-P. Dognon, *Coord. Chem. Rev.*, 2014, **266**, 110–122.

[41] E. Lu, S. Sajjad, V. E. Berryman, A. J. Wooles, N. Kaltsoyannis and S. T. Liddle, *Nat. Commun.*, 2019, **10**, 1–10.

[42] A. Kerridge, *Chem. Commun.*, 2017, **53**, 6685–6695.

[43] K. P. Carter, R. M. Pallares and R. J. Abergel, *Commun. Chem.*, 2020, **3**, 1–4.

[44] J. A. Platts and R. J. Baker, *Dalton Trans.*, 2020, **49**, 1077–1088.

[45] M. P. Kelley, J. Su, M. Urban, M. Luckey, E. Batista, P. Yang and J. C. Shafer, *J. Am. Chem. Soc.*, 2017, **139**, 9901–9908.

[46] B. Sadhu and M. Dolg, *Inorg. Chem.*, 2019, **58**, 9738–9748.

[47] M. Dolg, W. Liu and S. Kalvoda, *Int. J. Quantum Chem.*, 2000, **76**, 359–370.

[48] W.-X. Ji, W. Xu, W. H. E. Schwarz and S.-G. Wang, *J. Comput. Chem.*, 2015, **36**, 449–458.

[49] W. Xu, W.-X. Ji, Y.-X. Qiu, W. H. E. Schwarz and S.-G. Wang, *Phys. Chem. Chem. Phys.*, 2013, **15**, 7839–7847.

[50] N. Kaltsoyannis, *Inorg. Chem.*, 2013, **52**, 3407–3413.

[51] T. J. Duignan and J. Autschbach, *J. Chem. Theory Comput.*, 2016, **12**, 3109–3121.

[52] G. Kaindl, G. Wertheim, G. Schmiester and E. Sampathkumaran, *Phys, Rev. Lett.*, 1987, **58**, 606.

[53] G. Kaindl, G. Schmiester, E. Sampathkumaran and P. Wachter, *Phys. Rev. B*, 1988, **38**, 10174.

[54] M. D. Walter, C. H. Booth, W. W. Lukens and R. A. Andersen, *Organometallics*, 2009, **28**, 698–707.

[55] C. Booth, Y. Jiang, D. Wang, J. Mitchell, P. Tobash, E. Bauer, M. Wall, P. Allen, D. Sokaras, D. Nordlund, T.-C. Weng, M. Torrez and J. Sarrao, *Proc. Natl. Acad. Sci. U.S.A.*, 2012, **109**, 10205–10209.

[56] C. H. Booth, S. Medling, Y. Jiang, E. Bauer, P. Tobash, J. Mitchell, D. Veirs, M. Wall, P. Allen, J. Kas, D.Sokaras, D.Nordlund and T.-C.Weng, *J. Electron. Spectros. Relat. Phenomena*, 2014, **194**, 57–65.

[57] R. Bès, M. Rivenet, P.-L. Solari, K. O. Kvashnina, A. C. Scheinost and P. M. Martin, *Inorg. Chem.*, 2016, **55**, 4260–4270.

[58] T. Vitova, I. Pidchenko, D. Fellhauer, P. S. Bagus, Y. Joly, T. Pruessmann, S. Bahl, E. Gonzalez-Robles, J. Rothe, M. Altmaier, M. A. Denecke and H. Geckeis, *Nat. Commun.*, 2017, **8**, 16053.

[59] T. Vitova, I. Pidchenko, D. Fellhauer, T. Pruessmann, S. Bahl, K. Dardenne, T. Yokosawa, B. Schimmelpfennig, M. Altmaier, M. Denecke, J. Rothe and H. Geckeis, *Chem. Commun.*, 2018, **54**, 12824–12827.

[60] R. L. Halbach, G. Nocton, C. H. Booth, L. Maron and R. A. Andersen, *Inorg. Chem.*, 2018, **57**, 7290–7298.

[61] E. Epifano, M. Naji, D. Manara, A. C. Scheinost, C. Hennig, J. Lechelle, R. Konings, C. Guéneau, D. Prieur, T. Vitova, K. Dardenne, J. Rothe and P. M. Martin, *Commun. Chem.*, 2019, **2**, 1–11.

[62] T. Vitova, I. Pidchenko, D. Schild, T. Prüßmann, V. Montoya, D. Fellhauer, X. Gaona, E. Bohnert, J. Rothe, R. J. Baker and H. Geckeis, *Inorg. Chem.*, 2019, **59**, 8–22.

[63] G. Leinders, R. Bes, K. O. Kvashnina and M. Verwerft, *Inorg. Chem.*, 2020, **59**, 4576–4587.

[64] E. Gerber, A. Y. Romanchuk, I. Pidchenko, L. Amidani, A. Rossberg, C. Hennig, G. B. Vaughan, A. Trigub, T. Egorova, S. Bauters, T. Plakhova, M. O. J. Y. Hunault, S. Weiss, S. M. Butorin, A. C. Scheinost, S. N. Kalmykov and K. O. Kvashnina, *Nanoscale*, 2020, **12**, 18039–18048.

[65] E. Gerber, A. Y. Romanchuk, S. Weiss, S. Bauters, B. Schacherl, T. Vitova, R. Hübner, S. Shams Aldin Azzam, D. Detollenaere, D. Banerjee, S. M. Butorin, S. N. Kalmykov and K. O. Kvashnina, *Inorg. Chem. Front.*, 2021, **8**, 1102–1110.

[66] A. V. Soldatov, T. S. Ivanchenko, S. Della Longa, A. Kotani, Y. Iwamoto and A. Bianconi, *Phys. Rev. B*, 1994, **50**, 5074–5080.

[67] A. Soldatov, T. Ivanchenko, A. Kotani and A. Bianconi, *Physica B*, 1995, **208**, 53–55.

[68] A. Kotani, K. Kvashnina, S. M. Butorin and P. Glatzel, *Eur. Phys. J. B*, 2012, **85**, 257.

[69] D.-C. Sergentu, C. H. Booth and J. Autschbach, *Chem. Eur. J.*, 2021, **27**, 7239–7251.

[70] C. H. Booth, M. D. Walter, M. Daniel, W. W. Lukens and R. A. Andersen, *Phys. Rev. Lett.*, 2005, **95**, 267202.

[71] D.-C. Sergentu, T. J. Duignan and J. Autschbach, *J. Phys. Chem. Lett.*, 2018, **9**, 5583–5591.

[72] O. Bunau and Y. Joly, *J. Phys.: Condens. Matter*, 2009, **21**, 345501.

[73] Y. Joly, O. Bunau, J. E. Lorenzo, R. M. Galéra, S. Grenier and B. Thompson, *J. Phys. Conf. Ser.*, 2009, **190**, 012007.

[74] J. J. Rehr, J. J. Kas, F. D. Vila, M. P. Prange and K. Jorissen, *Phys. Chem. Chem. Phys.*, 2010, **12**, 5503–5513.

[75] K. Mathew, C. Zheng, D. Winston, C. Chen, A. Dozier, J. J. Rehr, S. P. Ong and K. A. Persson, *Sci. Data*, 2018, **5**, 1–8.

[76] K. O. Kvashnina, A. Y. Romanchuk, I. Pidchenko, L. Amidani, E. Gerber, A. Trigub, A. Rossberg, S. Weiss, K. Popa, O. Walter, R. Caciuffo, A. C. Scheinost, S. M. Butorin and S. N. Kalmykov, *Angew. Chem. Int. Ed.*, 2019, **58**, 17558–17562.

[77] L. Amidani, T. V. Plakhova, A. Y. Romanchuk, E. Gerber, S. Weiss, A. Efimenko, C. J. Sahle, S. M. Butorin, S. N. Kalmykov and K. O. Kvashnina, *Phys. Chem. Chem. Phys.*, 2019, **21**, 10635–10643.

[78] C. Fillaux, C. Den Auwer, D. Guillaumont, D. K. Shuh and T. Tyliszczak, *J. Alloys Compd.*, 2007, **444**, 443–446.

[79] C. Fillaux, D. Guillaumont, J.-C. Berthet, R. Copping, D. K. Shuh, T. Tyliszczak and C. Den Auwer, *Phys. Chem. Chem. Phys.*, 2010, **12**, 14253–14262.

[80] J. G. Tobin and D. Sokaras, *J. Vac. Sci. Technol. A*, 2020, **38**, 036001.

[81] H. Ågren, V. Carravetta, O. Vahtras and L. G. Pettersson, *Chem. Phys. Lett.*, 1994, **222**, 75–81.

[82] Y. Zhang, J. D. Biggs, D. Healion, N. Govind and S. Mukamel, *J. Chem. Phys.*, 2012, **137**, 194306.

[83] C. South, A. Shee, D. Mukherjee, A. K. Wilson and T. Saue, *Phys. Chem. Chem. Phys.*, 2016, **18**, 21010–21023.

[84] E. Stavitski and F. M. de Groot, *Micron*, 2010, **41**, 687–694.

[85] P. S. Bagus, H. Freund, H. Kuhlenbeck and E. S. Ilton, *Chem. Phys. Lett.*, 2008, **455**, 331–334.

[86] P. S. Bagus, B. Schacherl and T. Vitova, *Inorg. Chem.*, 2021, **60**, 16090–16102.

[87] N. A. Besley, *WIREs Comput. Mol. Sci.*, 2021, **11**, e1527.

[88] N. Govind and W. A. de Jong, *Theor. Chem. Acc.*, 2014, **133**, 1–7.

[89] Y. Qiao, G. Ganguly, C. H. Booth, J. A. Branson, A. S. Ditter, D. J. Lussier, L. M. Moreau, D. Russo, D.-C. Sergentu, D. K. Shuh, T. Sun, J. Autschbach and S. G. Minasian, *Chem. Commun.*, 2021, **57**, 9562–9565.

[90] M. Roemelt, D. Maganas, S. DeBeer and F. Neese, *J. Chem. Phys.*, 2013, **138**, 204101.

[91] M. Roemelt and F. Neese, *J. Phys. Chem. A*, 2013, **117**, 3069–3083.

[92] D. Maganas, M. Roemelt, M. Hävecker, A. Trunschke, A. Knop-Gericke, R. Schlögl and F. Neese, *Phys. Chem. Chem. Phys.*, 2013, **15**, 7260–7276.

[93] A. Kubas, M. Verkamp, J. Vura-Weis, F. Neese and D. Maganas, *J. Chem. Theory. Comput.*, 2018, **14**, 4320–4334.

[94] J. T. Lukens, I. M. DiMucci, T. Kurogi, D. J. Mindiola and K. M. Lancaster, *Chem. Sci.*, 2019, **10**, 5044–5055.

[95] E. B. Boydas, B. Winter, D. Batchelor and M. Roemelt, *Int. J. Quantum Chem*, 2021, **121**, e26515.

[96] M. Lundberg and M. G. Delcey, *Transition Metals in Coordination Environments*, Springer, 2019, pp. 185–217.

[97] S. I. Bokarev and O. Kühn, *WIREs Comput. Mol. Sci.*, 2020, **10**, e1433.

[98] F. M. de Groot, H. Elnaggar, F. Frati, R. pan Wang, M. U. Delgado-Jaime, M. van Veenendaal, J. Fernandez-Rodriguez, M. W. Haverkort, R. J. Green, G. van der Laan, Y. Kvashnin, A. Hariki, H. Ikeno, H. Ramanantoanina, C. Daul, B. Delley, M. Odelius, M. Lundberg, O. Kuhn, S. I. Bokarev, E. Shirley, J. Vinson, K. Gilmore, M. Stener, G. Fronzoni, P. Decleva, P. Kruger, M. Retegan, Y. Joly, C. Vorwerk, C. Draxl, J. Rehr and A. Tanaka, *J. Electron Spectrosc. Relat. Phenom.*, 2021, **249**, 147061.

[99] I. Josefsson, K. Kunnus, S. Schreck, A. Föhlisch, F. de Groot, P. Wernet and M. Odelius, *J. Phys. Chem. Lett.*, 2012, **3**, 3565–3570.

[100] P. Wernet, K. Kunnus, S. Schreck, W. Quevedo, R. Kurian, S. Techert, F. M. F. de Groot, M. Odelius and A. Föhlisch, *J. Phys. Chem. Lett.*, 2012, **3**, 3448–3453.

[101] K. Atak, S. I. Bokarev, M. Gotz, R. Golnak, K. M. Lange, N. Engel, M. Dantz, E. Suljoti, O. Kühn and E. F. Aziz, *J. Phys. Chem. B*, 2013, **117**, 12613–12618.

[102] S. I. Bokarev, M. Dantz, E. Suljoti, O. Kühn and E. F. Aziz, *Phys. Rev. Lett.*, 2013, **111**, 083002.

[103] S. Edlira, G.-D. Raul, S. I. Bokarev, K. M. Lange, R. Schoch, B. Dierker, M. Dantz, K. Yamamoto, N. Engel, K. Atak, O. Kühn, M. Bauer, J.-E. Rubensson and E. F. Aziz, *Angew. Chem. Int. Ed.*, 2013, **52**, 9841–9844.

[104] N. Engel, S. I. Bokarev, E. Suljoti, R. Garcia-Diez, K. M. Lange, K. Atak, R. Golnak, A. Kothe, M. Dantz, O. Kühn and E. F. Aziz, *J. Phys. Chem. B*, 2014, **118**, 1555–1563.

[105] C. J. Pollock, M. U. Delgado-Jaime, M. Atanasov, F. Neese and S. DeBeer, *J. Am. Chem. Soc.*, 2014, **136**, 9453–9463.

[106] R. V. Pinjari, M. G. Delcey, M. Guo, M. Odelius and M. Lundberg, *J. Chem. Phys.*, 2014, **141**, 124116.

[107] D. Maganas, P. Kristiansen, L.-C. Duda, A. Knop-Gericke, S. DeBeer, R. Schlögl and F. Neese, *J. Phys. Chem. C*, 2014, **118**, 20163–20175.

[108] S. I. Bokarev, M. Khan, M. K. Abdel-Latif, J. Xiao, R. Hilal, S. G. Aziz, E. F. Aziz and O. Kühn, *J. Phys. Chem. C*, 2015, **119**, 19192–19200.

[109] G. Grell, S. I. Bokarev, B. Winter, R. Seidel, E. F. Aziz, S. G. Aziz and O. Kühn, *J. Chem. Phys.*, 2015, **143**, 074104.

[110] N. C. Tomson, K. D. Williams, X. Dai, S. Sproules, S. DeBeer, T. H. Warren and K. Wieghardt, *Chem. Sci.*, 2015, **6**, 2474–2487.

[111] R. V. Pinjari, M. G. Delcey, M. Guo, M. Odelius and M. Lundberg, *J. Comput. Chem*, 2016, **37**, 477–486.

[112] M. Preuße, S. I. Bokarev, S. G. Aziz and O. Kühn, *Struct. Dyn.*, 2016, **3**, 062601.

[113] A. Chantzis, J. K. Kowalska, D. Maganas, S. DeBeer and F. Neese, *J. Chem. Theory Comput.*, 2018, **14**, 3686–3702.

[114] D. Maganas, J. K. Kowalska, M. Nooijen, S. DeBeer and F. Neese, *J. Chem. Phys.*, 2019, **150**, 104106.

[115] B. H. Allehyani, W. I. Hassan, S. G. Aziz, R. H. Hilal, O. Kühn and S. I. Bokarev, *Chem. Phys.*, 2020, **532**, 110681.

[116] G. Ganguly, D.-C. Sergentu and J. Autschbach, *Chem. Eur. J.*, 2020, **26**, 1776–1788.

[117] B. O. Roos, P. R. Taylor and P. E. M. Siegbahn, *Chem. Phys.*, 1980, **48**, 157–173.

[118] J. Olsen, B. O. Roos, P. Jørgensen and H. J. A. Jensen, *J. Chem. Phys.*, 1988, **89**, 2185–2192.

[119] P. Å. Malmqvist, A. Rendell and B. O. Roos, *J. Phys. Chem.*, 1990, **94**, 5477–5482.

[120] R. Polly, B. Schacherl, J. Rothe and T. Vitova, *Inorg. Chem.*, 2021, DOI: 10.1021/acs.inorgchem.1c02364.

[121] J. Finley, P.-Å. Malmqvist, B. O. Roos and L. Serrano-Andrès, *Chem. Phys. Lett.*, 1998, **288**, 299–306.

[122] K. Andersson, P.-Å. Malmqvist, B. O. Roos, A. J. Sadlev and K. Wolinski, *J. Phys. Chem.*, 1990, **94**, 5483–5488.

[123] K. Andersson and B. O. Roos, *Chem. Phys. Lett.*, 1992, **191**, 507–514.

[124] P. Å. Malmqvist, K. Pierloot, A. R. M. Shahi, C. J. Cramer and L. Gagliardi, *J. Chem. Phys.*, 2008, **128**, 204109.

[125] C. Angeli, R. Cimiraglia, S. Evangelisti, T. Leininger and J.-P. Malrieu, *J. Chem. Phys.*, 2001, **114**, 10252–10264.

[126] P.-A. Malmqvist, B. O. Roos and B. Schimmelpfennig, *Chem. Phys. Lett.*, 2002, **357**, 230–240.

[127] F. Gendron, D. Páez-Hernández, F.-P. Notter, B. Pritchard, H. Bolvin and J. Autschbach, *Chem. Eur. J.*, 2014, **20**, 7994–8011.

[128] J. Autschbach, *Comments Inorg. Chem.*, 2016, **36**, 215–244.

[129] F. Gendron, B. Le Guennic and J. Autschbach, *Inorg. Chem.*, 2014, **53**, 13174–13187.

[130] F. Gendron, H. Bolvin and J. Autschbach, *Organometallic Magnets*, Springer, Berlin, Heidelberg, 2018, vol. 64, pp. 355–390.

[131] I. F. Galván, M. Vacher, A. Alavi, C. Angeli, F. Aquilante, J. Autschbach, J. J. Bao, S. I. Bokarev, N. A. Bogdanov, R. K. Carlson, L. F. Chibotaru, J. Creutzberg, N. Dattani, M. G. Delcey, S. Dong, A. Dreuw, L. Freitag, L. M. Frutos, L. Gagliardi, F. Gendron, A. Giussani, L. Gonzalez, G. Grell, M. Guo, C. E. Hoyer, M. Johansson, S. Keller, S. Knecht, G. Kovačević, E. Källman, G. Li Manni, M. Lundberg, Y. Ma, S. Mai, J. P. Malhado, P. A. Malmqvist, P. Marquetand, S. A. Mewes, J. Norell, M. Olivucci, M. Oppel, Q. M. Phung, K. Pierloot, F. Plasser, M. Reiher, A. M. Sand, I. Schapiro, P. Sharma, C. J. Stein, L. K. Sørensen, D. G. Truhlar, M. Ugandi, L. Ungur, A. Valentini, S. Vancoillie, V. Veryazov, O. Weser, T. A. Wesołowski, P.-O. Widmark, S. Wouters, A. Zech, J. P. Zobel and R. Lindh, *J. Chem. Theory Comput.*, 2019, **15**, 5925–5964.

[132] F. Aquilante, J. Autschbach, A. Baiardi, S. Battaglia, V. A. Borin, L. F. Chibotaru, I. Conti, L. De Vico, M. Delcey, I. Fdez. Galván, N. Ferré, L. Freitag, M. Garavelli, X. Gong, S. Knecht, E. D. Larsson, R. Lindh, M. Lundberg, P. Å. Malmqvist, A. Nenov, J. Norell, M. Odelius, M. Olivucci, T. B. Pedersen, L. Pedraza-González, Q. M. Phung, K. Pierloot, M. Reiher, I. Schapiro, J. Segarra-Martí, F. Segatta, L. Seijo, S. Sen, D.-C. Sergentu, C. J. Stein, L. Ungur, M. Vacher, A. Valentini and V. Veryazov, *J. Chem. Phys.*, 2020, **152**, 214117 (25 pages).

[133] A. Marchenko, T. Duignan, A. Philips, T. G. Badger, H. D. Ludowieg and B. Moore, *Exatomic: A unified platform for computational chemists*, `https://github.com/exa-analytics/exatomic`, DOI: 10.5281/zenodo.1256873. Accessed 11/21.

[134] E. D. Glendening, C. R. Landis and F. Weinhold, *Wiley Interdiscip. Rev.: Comput.Mol. Sci.*, 2012, **2**, 1–42.

[135] E. D. Glendening, C. R. Landis and F. Weinhold, *J. Comput. Chem*, 2019, **40**, 2234–2241.

[136] R. L. Martin, *J. Chem. Phys.*, 2003, **118**, 4775–4777.

[137] I. Mayer, *Chem. Phys. Lett.*, 2007, **437**, 284–286.

[138] F. Plasser, M. Wormit and A. Dreuw, *J. Chem. Phys.*, 2014, **141**, 024106.

[139] P. Å. Malmqvist and V. Veryazov, *Mol. Phys.*, 2012, **110**, 2455–2464.

[140] R. Feng, X. Yu and J. Autschbach, *J. Chem. Theory Comput.*, 2021, **17**, 7531–7544.

[141] A. Streitwieser Jr and N. Yoshida, *J. Am. Chem. Soc.*, 1969, **91**, 7528–7528.

[142] A. Streitwieser Jr and U. Mueller-Westerhoff, *J. Am. Chem. Soc.*, 1968, **90**, 7364–7364.

[143] J. P. Clark and J. C. Green, *J. Organomet. Chem*, 1976, C14–C16.

[144] J. P. Clark and J. C. Green, *J. Chem. Soc., Dalton Trans.*, 1977, 505–508.

[145] A. Kerridge and N. Kaltsoyannis, *J. Phys. Chem. A*, 2009, **113**, 8737–8745.

[146] A. Kerridge, *Dalton Trans.*, 2013, **42**, 16428–16436.

[147] J. S. Parry, F. G. N. Cloke, S. J. Coles and M. B. Hursthouse, *J. Am. Chem. Soc.*, 1999, **121**, 6867–6871.

[148] M. P. Kelley, I. A. Popov, J. Jung, E. R. Batista and P. Yang, *Nat. Commun.*, 2020, **11**, 1–10.

[149] B. O. Roos, A. C. Borin and L. Gagliardi, *Angew. Chem. Int. Ed.*, 2007, **46**, 1469–1472.

[150] M. Pepper and B. E. Bursten, *Chem. Rev.*, 1991, **91**, 719–741.

[151] K. G. Dyall, *Mol. Phys.*, 1999, **96**, 511–518.

[152] R. G. Denning, J. C. Green, T. E. Hutchings, C. Dallera, A. Tagliaferri, K. Giarda, N. B. Brookes and L. Braicovich, *J. Chem. Phys.*, 2002, **117**, 8008–8020.

[153] S. Matsika, Z. Zhang, S. R. Brozell, J.-P. Blaudeau, Q. Wang and R. M. Pitzer, *J. Phys. Chem. A*, 2001, **105**, 3825–3828.

[154] P. J. Hay, R. L. Martin and G. Schreckenbach, *J. Phys. Chem. A*, 2000, **104**, 6259–6270.

[155] G. A. Shamov and G. Schreckenbach, *J. Phys. Chem. A*, 2005, **109**, 10961–10974.

[156] E. Varathan, Y. Gao and G. Schreckenbach, *J. Phys. Chem. A*, 2021, **125**, 920–932.

[157] D. Rios, M. del Carmen Michelini, A. F. Lucena, J. Marcalo and J. K. Gibson, *J. Am. Chem. Soc.*, 2012, **134**, 15488–15496.

[158] A. F. Lucena, S. O. Odoh, J. Zhao, J. Marcalo, G. Schreckenbach and J. K. Gibson, *Inorg. Chem.*, 2014, **53**, 2163–2170.

[159] N. Kaltsoyannis, *Dalton Trans.*, 2016, **45**, 3158–3162.

[160] A. Streitwieser, S. A. Kinsley, J. T. Rigsbee, I. L. Fragala and E. Ciliberto, *J. Am. Chem. Soc.*, 1985, **107**, 7786–7788.

[161] M. Dolg, P. Fulde, W. Küchle, C.-S. Neumann and H. Stoll, *J. Chem. Phys.*, 1991, **94**, 3011–3017.

[162] M. Dolg, P. Fulde, H. Stoll, H. Preuss, A. Chang and R. M. Pitzer, *Chem. Phys.*, 1995, **195**, 71–82.

[163] N. M. Edelstein, P. Allen, J. Bucher, D. Shuh, C. Sofield, N. Kaltsoyannis, G. Maunder, M. Russo and A. Sella, *J. Am. Chem. Soc.*, 1996, **118**, 13115–13116.

[164] M. Dolg and P. Fulde, *Chem. - A Eur. J.*, 1998, **4**, 200–204.

[165] A. Streitwieser, S. A. Kinsley, C. H. Jenson and J. T. Rigsbee, *Organometallics*, 2004, **23**, 5169–5175.

[166] A. Kerridge, R. Coates and N. Kaltsoyannis, *J. Phys. Chem. A*, 2009, **113**, 2896–2905.

[167] O. Mooßen and M. Dolg, *Chem. Phys. Lett.*, 2014, **594**, 47–50.

[168] A. Kotani, *Mod. Phys. Lett. B*, 2013, **27**, 1330012.

[169] S. Coriani and H. Koch, *J. Chem. Phys.*, 2015, **143**, 181103.

[170] R. H. Myhre, S. Coriani and H. Koch, *J. Chem. Theory Comput.*, 2016, **12**, 2633–2643.

[171] M. L. Vidal, X. Feng, E. Epifanovsky, A. I. Krylov and S. Coriani, *J. Chem. Theory Comput.*, 2019, **15**, 3117–3133.

[172] F. Frati, F. de Groot, J. Cerezo, F. Santoro, L. Cheng, R. Faber and S. Coriani, *J. Chem. Phys.*, 2019, **151**, 064107.

[173] M. L. Vidal, P. Pokhilko, A. I. Krylov and S. Coriani, *J. Phys. Chem. Lett.*, 2020, **11**, 8314–8321.

[174] Center for Computational Research, University at Buffalo. URL `http://hdl.handle.net/10477/79221`. Accessed 11/2019.